
Article:
Wang, J.B., Jewell, G.W. and Howe, D. (1997) A novel spherical actuator: Design and control. IEEE Transactions on Magnetics, 33 (5 (Par). pp. 4209-4211. ISSN 0018-9464

https://doi.org/10.1109/20.619712

A Novel Spherical Actuator: Design and Control

Jiabin Wang, Geraint W. Jewell and David Howe
Department of Electronic and Electrical Engineering, University of Sheffield, Mappin Street, Sheffield, S1 3JD, U.K.

Abstract — **The paper describes the design and control of a novel spherical permanent magnet actuator which is capable of two-degrees-freedom and a high specific torque. Based on an analytical actuator model, an optimal design procedure is developed to yield maximum output torque or maximum system acceleration for a given payload. The control of the actuator, whose dynamics are similar to those of robotic manipulators, is facilitated by the establishment of a complete actuation system model. A robust control law is applied, and its effectiveness is demonstrated by computer simulation.**

I. Introduction

Recent advances in robotics, office automation, and intelligent flexible manufacturing and assembly systems have necessitated the development of precision multiple degree-of-freedom actuation systems. In general, however, motion with several degrees of freedom is realized almost exclusively by the use of a separate motor/actuator for each axis, which results in complicated transmission systems and relatively heavy structures. Thus, it is difficult to achieve a high dynamic performance, due to the effects of inertia, backlash, non-linear friction, and elastic deformation of gears. Actuators which are capable of controlled motion in two or more degrees-of-freedom can alleviate the problem, whilst being lighter and more efficient. However, although such actuators have been the subject of some research [1]-[3], they have rarely been commercialized, due to their complexity, and related difficulties in modelling their electromagnetic behaviour and optimizing their design.

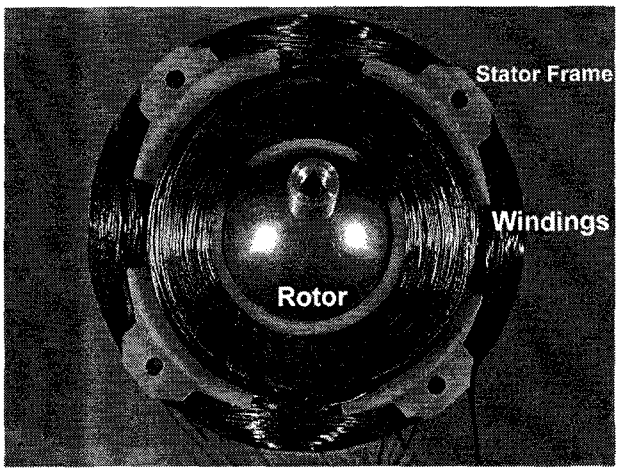

Fig. 1 Spherical actuator

Fig. 1 shows a prototype of a new form of actuator with a spherical permanent magnet rotor and a simple stator winding arrangement [4],[5]. It is capable of two degrees-of-freedom and a high specific torque, whilst having a robust mechanical structure and a simple position sensing system. The spherical rotor is housed within the spherical stator on a low friction surface coating. Accommodated on the stator are three orthogonal windings, which may be enclosed by an outer spherical iron shell in order to increase the flux-linkage. The 2-pole rare-earth permanent magnet rotor, may either be solid or hollow, when it may include an inner spherical iron core, and can be either diametrically or radially magnetized. On the application of current to the stator windings, the resulting torque will orientate the rotor to minimize the system potential energy. Thus, control of the rotor orientation is achieved by varying the winding currents. This paper addresses the design and control aspects of the actuator, for which a detailed analysis and system model is described in [4],[5]

Manuscript received January 25, 1997
J. Wang, +44 114 2225898, fax +44 114 2225196, J.B.Wang@shef.ac.uk

II. Design Optimization

Due to the simplicity of the actuator topology, the magnetic field distribution, and torque vector and back-emf constant can be derived analytically[4]. This allows for the design of the actuator to be optimized with respect to a given criterion. The prime considerations in this paper are either maximum torque capability or maximum achievable acceleration with a given payload, although other criteria, e.g. minimum cost, may similarly be addressed.

A. Maximum Output Torque Design

Without loss of generality, an air-cored spherical actuator is assumed. Its electromagnetic torque is given by [4]:

$$T_{em} = T_{m0} R_s^4 x_r^3 \left(1 - x_r - G_p / R_s\right) \quad (1)$$

where x_r is equivalent to the split ratio of conventional permanent magnet machines, and is the ratio of the rotor radius R_m to the outer radius of the stator R_s, and G_p is the airgap length. T_{m0} is a constant related to the remanence of the magnet, B_{rem}, the winding current density, J, the packing factor, P_f, and the winding geometrical angles, δ_1 and δ_0, and is given by:

$$T_{m0} = 2\pi P_f B_{rem} J(\delta_1 - \delta_0 + 0.5(\sin 2\delta_0 - \sin 2\delta_1))/3 \quad (2)$$

As has been shown [4], for a given R_s, there is an optimal split ratio, viz. $x_r = 3(1-G_p/R_s)/4$, which yields maximum torque. This result is obtained when friction-free conditions are assumed. In the present actuator, the rotor magnet is in direct contact with the stator housing, and the friction torque is, therefore, not negligible, although it can be minimized by using a low friction coating or a lubricant. Over the range of

rotor operating speeds, Coulomb friction, which is proportional to the rotor weight, is a dominant factor, and is given by:

$$T_f = 4\pi\rho R_m^4 g f_c / 3 \tag{3}$$

where f_c is the Coulomb friction coefficient, ρ is the mass density of the magnet and g is the gravitational acceleration. The effective output torque of the actuator can, therefore, be written as:

$$T_{eff} = T_{em} - T_f = R_s^4 x_r^3 \left(T_{m0}\left(b - x_r\right) - c x_r\right) \tag{4}$$

where $b = (1 - G_p/R_s)$ and $c = 4\pi\rho g f_c/3$. It is evident that the optimal value of the ratio x_r is:

$$x_r = 3T_{m0} b / 4(T_{m0} + c) \tag{5}$$

Fig. 2 shows T_{em} and T_{eff} as functions of x_r, assuming R_s = 0.036[m], B_{rem} = 1.2 [T], J = 4.0 [A/mm^2], P_f=0.5, δ_1= 0.6208 [rad], δ_0 = 0.1222[rad], g = 9.8 [m/s^2], ρ = 7.5x10^3 [kg/m^3] and f_c = 0.12. As is seen, the effective output torque is reduced by an amount corresponding to the friction torque, which is proportional to x_r^4. Consequently, the optimal split ratio x_r is reduced, compared with the optimal friction-free value. Since the optimal value of x_r is proportional to $(1 - G_p/R_s)$, it decreases as R_s decreases and approaches $3T_{m0}/4(T_{m0}+c)$ as R_s increases, provided that $G_p/R_s << 1$.

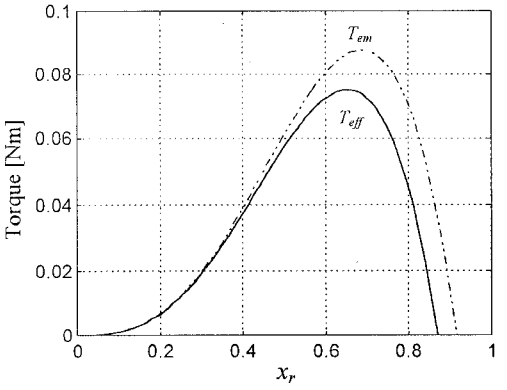

Fig. 2 Torque vs. $x_r = R_m/R_s$ curves

B. Maximum Acceleration Design

A common requirement is for maximum acceleration from an actuator so as to achieve the fastest dynamic response for a given payload. Assuming that the payload can be approximated by a point mass, m_c, with its center of gravity at $r_c = R_s + l_c$, then the additional inertia I_c , friction torque T_{fc} and gravitational torque T_g , due to the payload, are given, respectively, by:

$$I_c = m_c r_c^2 \ ; \ T_{fc} = m_c g R_m f_c \ ; \ T_g = m_c g r_c \tag{6}$$

The maximum attainable acceleration, when a pair of diametrically opposite windings is excited, is:

$$\begin{aligned} A_{eff} &= \left(T_{em} - (T_f + T_{fc} + T_g)\right) / (I_r + I_c) \\ &= \frac{R_s^4 x_r^3 \left(T_{m0}\left(b - x_r\right) - c x_r\right) - m_c g (r_c + f_c R_s x_r)}{8\rho\pi R_s^5 x_r^5 / 15 + m_c (r_c)^2} \end{aligned} \tag{7}$$

For a given R_s, the optimal value of x_r is obtained from the solution of the following equations:

$$\begin{cases} a_8 x_r^8 + a_7 x_r^7 + a_5 x_r^5 + a_4 x_r^4 + a_3 x_r^3 + a_2 x_r^2 + a_0 = 0 \\ 0 < x_r < 1 \end{cases} \tag{8}$$

where

$$a_8 = c_1 (T_{m0} + c) R_s^8 \ ; \ a_7 = -2 c_1 T_{m0} b R_s^8 \ ; \ a_5 = 4 c_1 m_c g f_c R_s^5$$
$$a_4 = 5 c_1 m_c g r_c R_s^4 \ ; \ a_3 = -4 (T_{m0} + c) I_c R_s^3 \ ; \ a_2 = 3 T_{m0} b I_c R_s^3$$
$$a_0 = -m_c g f_c I_c \ ; \ c_1 = 8\pi\rho / 15$$

Equation (8) may be solved numerically, e.g., using the Matlab routine *Roots*. Fig. 3 shows the maximum acceleration, as a function of R_s and x_r assuming m_c=0.05 [kg], l_c = 0.017[m], which correspond to a payload such as a miniature high resolution electronic camera, the other parameters being the same as those specified earlier. At R_s = 0.036[m], the corresponding optimal split ratio x_r is 0.583, which is lower than the optimal value for maximum output torque. As can be seen from Fig. 3, the optimal ratio decreases slightly as R_s increases. This is due to the fact that the electromagnetic torque increases with R_s^4 whilst the moment of inertia of the rotor increases with R_m^5. Thus, in order to maintain maximum acceleration, any increase in the value of R_m should be proportionally less than any increase of R_s.

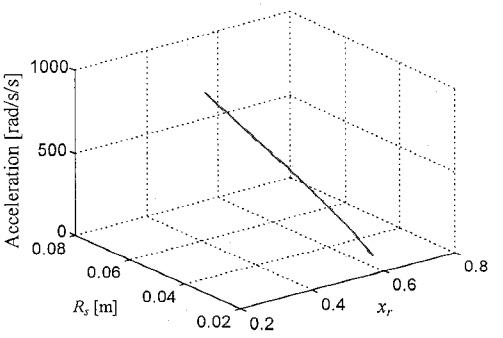

Fig. 3 Maximum acceleration as a function of R_s and x_r

Based on the above results, an integrated design procedure can be formulated to yield optimal designs in terms of a chosen criterion for a given specification.

III. Control of Spherical Actuator

A complete dynamic model for the actuator is given by[5]:

$$\begin{cases} \boldsymbol{M}\ddot{\boldsymbol{Q}}_E + \boldsymbol{C}\dot{\boldsymbol{Q}}_E + \boldsymbol{G} + \tau_{fE} = \boldsymbol{K}_{ET}\boldsymbol{i}_w \\ \boldsymbol{L}\dot{\boldsymbol{i}}_w + \boldsymbol{R}\boldsymbol{i}_w - \boldsymbol{K}_{ET}^T\dot{\boldsymbol{Q}}_E = \boldsymbol{u}_E \end{cases} \tag{9}$$

where $\boldsymbol{Q}_E = [\beta\ \alpha]^T$ are the Euler angles representing the rotor orientation, the inertia matrix $\boldsymbol{M}$, the Coriolis and centripetal force matrix $\boldsymbol{C}$, and the gravitational torque vector $\boldsymbol{G}$ being given by:

$$\boldsymbol{M} = I_b\begin{bmatrix}(c\alpha)^2 & 0\\ 0 & 1\end{bmatrix};\boldsymbol{C} = I_b c\alpha s\alpha\begin{bmatrix}-\dot{\alpha} & -\dot{\beta}\\ \dot{\beta} & 0\end{bmatrix};\boldsymbol{G} = r_c m_c g\begin{bmatrix}-c\beta c\alpha\\ s\beta s\alpha\end{bmatrix}$$

where a shorthand notation for sine and cosine functions is used for clarity, e.g., sα represents for sinα. I_b is the combined moment of inertia of the rotor and payload referred in the rotor co-ordinate system, $\boldsymbol{u}_E = [u_A\ u_B\ u_C]^T$ is the winding terminal voltage vector, $\boldsymbol{i}_w = [i_A\ i_B\ i_C]^T$ is the winding current vector, $\boldsymbol{L}$ = diag$[L_A\ L_B\ L_C]^T$ is the diagonal winding self-inductance matrix, $\boldsymbol{R}$ = diag $[R_A\ R_B\ R_C]^T$ is the diagonal winding resistance matrix, τ_{fE} is the vector representing the Coulomb and viscous friction, and $\boldsymbol{K}_{ET}$, defined as the actuator torque matrix, is related to the actuator torque constant K_T [4] by:

$$\boldsymbol{K}_{ET} = K_T\begin{bmatrix}-s\beta c\alpha & 0 & -c\beta c\alpha\\ -c\beta s\alpha & c\alpha & s\beta s\alpha\end{bmatrix} \qquad (10)$$

Note that (9) has a singularity at $\alpha = 90^0$. However, with the present actuator design the angular excursion of α is within ± 45^0, and this singular point will never be encountered. Also, it will be noted that in non-singular regions, (9) constitutes a Hamiltonian system, and, therefore, possesses a well-understood structure and similar important properties as the dynamic equations for robotic manipulators. As a result, any advanced control law for the control of robotic manipulators can be applied to the spherical actuator.

As an example, a robust outer PD position control law [6] in conjunction with an inner PI current control law, as shown in Fig. 4, is utilized for the control of the spherical actuator. The role of the inner current tracking loop is to minimize the effects of back-emf and current transients on the outer position servo loop, so that a robust design philosophy [6] can be used to determine the control gain matrices $\boldsymbol{K}_V$ and Λ. The output of the position controller is two independent torque demands, but (9) has three independent control inputs. The extra degree of freedom in the control variables suggests that there exists a redundant control input which may be used for optimal control, e.g., to minimize the total energy consumption for a given torque demand. This control strategy is implemented by taking the weighted pseudo inverse of $\boldsymbol{K}_{ET}$, as denoted by $\boldsymbol{K}^+_{ET}$ in Fig. 4.

The effectiveness of this control strategy has been tested by computer simulation, in which all significant dynamic components, such as non-linear friction, saturation limits, quantization, and the sampling effect of digital control, are taken into account. Fig. 5 shows the simulated tracking error response to the input demand given by:

$$\beta = 0.7(1-e^{-50t^2});\ \alpha = 0.8(1-e^{-50t^2}) \qquad (11)$$

with 1(ms) sampling interval and $\boldsymbol{K}_V$ = diag [0.1 0.1], Λ= diag [100 100], I_b = 0.00014(kgm^2), K_T = 0.3 (Nm/A), $\boldsymbol{L}$ = diag [4.92 14.65 14.65] (mH) and $\boldsymbol{R}$ = diag [9.84 18.3 18.3] (Ω). As is seen, the actuator is able to track the input demand with good accuracy. The maximum tracking error is 0.0025 (rad) which occurs at 0.11(s). The tracking errors are not, however, zero even in the steady state, due to the presence of friction torque.

IV. Conclusions

A design methodology for a spherical permanent magnet actuator to achieve maximum output torque or maximum acceleration has been developed, and a control strategy for the closed-loop actuation system has been described. The stability and performance of this control strategy is guaranteed through the properties of its dynamic equations, and has been further verified by realistic computer simulation.

References

[1] K. Davey, G. Vachtsevanos and R. Powers, "The analysis of fields and torques in spherical induction motors" *IEEE Trans. on Magn*, vol. 23, pp. 273-282, 1987.

[2] K. Lee and C. Kwan , "Design concept development of a spherical stepper for robotic applications" *IEEE Trans. on Robot. Automat.*, vol. 7, pp. 175-181, 1991.

[3] B. Bederson, R. Wallace and E. Schwartz, "A miniature pan-tilt actuator: the spherical pointing motor" *IEEE Trans. on Robot. Automat.*, vol. 10, pp 298-308, 1994.

[4] J. Wang, G. W. Jewell and D. Howe, "Analysis of a spherical permanent magnet actuator" *J. Appl. Phys*, in press, 1997

[5] J. Wang, G. W. Jewell and D. Howe, "Modelling of a novel spherical permanent magnet actuator" *Proc. of IEEE Inter Conf. on Robotics and Automation*, New Mexico, U.S.A, in press, 1997,.

[6] J. Wang, S. J. Dodds and W.N. Bailey, "Guaranteed rates of convergence of a class of PD controllers for trajectory tracking problems of robotic manipulators with dynamic uncertainties" *IEE Proc.-Control Theory Appl.*, vol. 143, pp 186-190, 1996

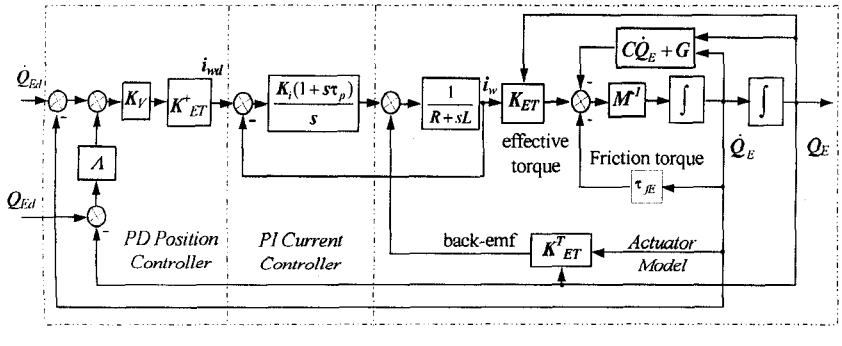

Fig. 4 Block diagram of closed -loop control system

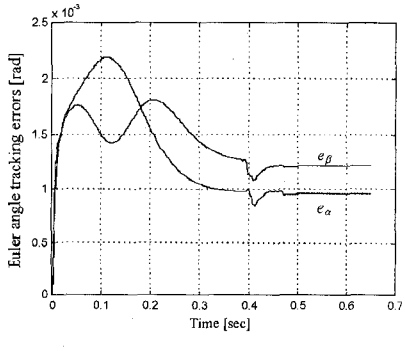

Fig. 5 Euler angle tracking error response